Quantification of reaction cycle parameters for an essential molecular switch in an auxin-responsive transcription circuit in rice

Lucila Andrea Acevedo[a], Jeahoo Kwon[a], and Linda K. Nicholson[a,1]

[a]Department of Molecular Biology and Genetics, Cornell University, Ithaca, NY 14853

Edited by G. Marius Clore, National Institute of Diabetes and Digestive and Kidney Diseases, National Institutes of Health, Bethesda, MD, and approved December 31, 2018 (received for review October 2, 2018)

Protein-based molecular switches play critical roles in biological processes. The importance of the prolyl *cis*–*trans* switch is underscored by the ubiquitous presence of peptidyl prolyl isomerases such as cyclophilins that accelerate the intrinsically slow isomerization rate. In rice, a tryptophan–proline (W-P) *cis*–*trans* switch in transcription repressor protein OsIAA11 along with its associated cyclophilin LRT2 are essential components in a negative feedback gene regulation circuit that controls lateral root initiation in response to the plant hormone auxin. Importantly, no quantitative characterizations of the individual (microscopic) thermodynamic and kinetic parameters for any cyclophilin-catalyzed W-P isomerization have been reported. Here we present NMR studies that determine and independently validate these parameters for LRT2 catalysis of the W-P motif in OsIAA11, providing predictive power for understanding the role of this switch in the auxin-responsive circuit and the resulting lateral rootless phenotype in rice. We show that the observed isomerization rate is linearly dependent on LRT2 concentration but is independent of OsIAA11 concentration over a wide range, and LRT2 is optimally tuned to maintain OsIAA11 at its *cis*–*trans* equilibrium to supply the slower downstream *cis*-specific proteasomal degradation with maximal OsIAA11 substrate. This indicates that accelerating the LRT2-catalyzed isomerization would not accelerate OsIAA degradation, whereas decreasing this rate via targeted mutation could reveal relationships between circuit dynamics and lateral root development. Moreover, we show that sequences flanking the highly conserved Aux/IAA W-P motif do not impact LRT2 catalysis, suggesting that the parameters determined here are broadly applicable across highly conserved cyclophilins and their Aux/IAA targets.

OsIAA11 | LRT2 | degron motif | W-P prolyl isomerization | auxin circuit

Peptidyl prolyl *cis*–*trans* isomerase (PPIase) enzymes are found across living organisms, from bacteria to humans (1–4). These enzymes accelerate the rate of exchange between *cis* and *trans* isomers of X-Pro (X-P) peptide bonds in target proteins, where X is any amino acid residue. While the role of this class of enzymes was initially thought to be limited to protein folding, their functional importance in a broad array of biological processes, including signal transduction, intracellular trafficking, gene transcription, cell cycle regulation, refolding of aggregated proteins, and regulation of reactive oxygen species by scavenging systems, is now convincingly demonstrated (3–7). Notably, a key way that a PPIase can regulate a biological pathway is to function as a molecular timer (4). For plant cyclophilins, thus far, their cellular functions have been shown to be essential in stress survival and the initiation of lateral root development (8, 9).

For the amino acid Pro, the backbone torsion angle ω can be either 0° (*cis*) or 180° (*trans*). Proline is unique in its ability to adopt the *cis* isomer due to its closed ring sidechain structure that brings the *cis* and *trans* isomers of the peptide bond much closer in free energy (10). For Pro in free peptides in aqueous solution, the *cis* isomer can exist at populations up to ∼50%, while the remaining 19 amino acids are almost exclusively in *trans* (5). Because the transition energy barrier between *cis* and *trans* states is large, in the absence of PPIases, the isomerization of the peptidyl prolyl bond is relatively slow, with a time constant on the order of minutes (11). PPIase activity can shorten this time constant by up to approximately five orders of magnitude (12), bringing it into the microsecond-to-millisecond regime that is typical for many types of cellular signaling events (13). The *cis*–*trans* equilibrium of a prolyl peptide bond can operate as a binary molecular switch, since, in principle, the structurally distinct *cis* and *trans* states can have different binding partners.

A striking example of isomer-specific binding is the recognition by the SCF^{TIR1} complex of the *cis* isomer of a specific and highly conserved tryptophan–proline (W-P) peptide bond in Aux/IAA proteins (14). The SCF^{TIR1} is an E3 ligase that ubiquitinates numerous Aux/IAA proteins in plants. Aux/IAA proteins are transcription repressors that play central roles in gene transcription circuits responsive to the phytohormone auxin (15, 16) that regulates many developmental processes in plants (17). Aux/IAA proteins contain a highly conserved GWPPV "degron motif" that binds only in the *cis* W-P isomer (WP^{cis}) to form a ternary complex with SCF^{TIR1} and auxin (14), resulting in subsequent polyubiquitination and degradation of Aux/IAA proteins via the proteasomal pathway (18). Since only WP^{cis} is polyubiquitinated and subsequently degraded, a PPIase is required for maintaining the equilibrium *cis* and *trans* populations as

Significance

The two-state nature (*cis* and *trans*) of the peptide bond between any amino acid residue and proline provides a bimodal switch with an intrinsically slow flipping rate. The *cis*–*trans* exchange rate is accelerated by isomerase enzymes, bringing this protein switch into relevant timescales for biological signaling. Turning on and off the expression of specific genes in response to hormone signals is a critical aspect of organism development. In rice, the initiation of lateral root development requires a prolyl *cis*–*trans* switch and its associated isomerase. Knowledge of the parameters that define this catalyzed reaction provides important predictive power for understanding the impact of this molecular switch as a timing device in a developmental process, and has broad implications across conserved systems.

Author contributions: L.A.A. and L.K.N. designed research; L.A.A. and J.K. performed research; L.A.A. and J.K. contributed new reagents/analytic tools; L.A.A. analyzed data; and L.A.A. and L.K.N. wrote the paper.

The authors declare no conflict of interest.

This article is a PNAS Direct Submission.

[1]To whom correspondence should be addressed. Email: lkn2@cornell.edu.

This article contains supporting information online at www.pnas.org/lookup/suppl/doi:10.1073/pnas.1817038116/-/DCSupplemental.

Published online January 29, 2019.

WP^{cis} is depleted, and thus for reducing the total Aux/IAA protein level. In the auxin-responsive circuit, an Aux/IAA protein binds to and inhibits an auxin-responsive factor (ARF) transcription activator on the targeted auxin-responsive promoter (19). When auxin appears, Aux/IAA protein is degraded by the proteasome, releasing ARF repression and activating transcription of the targeted genes, including the gene encoding the Aux/IAA protein (14–16, 18, 20). The activated expression of the Aux/IAA protein again leads to repression, thereby generating a classic negative feedback circuit (15, 16, 19, 21, 22). Hence, PPIase-catalyzed prolyl *cis–trans* isomerization of the W-P degron motif plays a critical role in controlling the level of Aux/IAA proteins involved in negative feedback circuits, where Aux/IAA proteins repress transcription of distinct sets of genes (including their own) involved in specific developmental pathways (18, 23, 24).

In rice, OsIAA11 is an Aux/IAA protein that regulates lateral root initiation (25). Recently, the cyclophilin LRT2 was also shown to be essential for lateral root development (9, 26). Convincing evidence supports a key regulatory role of LRT2 in the OsIAA11-controlled auxin-responsive circuit (27). Specifically, in LRT2 knockout rice plants (*lrt2*$^{-/-}$), the accumulation of OsIAA11 is increased and lateral root formation is suppressed relative to WT plants, and RNAi knockdown of OsIAA11 in *lrt2*$^{-/-}$ plants partially restores lateral root formation (27). Moreover, incubation of recombinant His-OsIAA11 with protein extracts from WT or *lrt2*$^{-/-}$ plants shows that LRT2 promotes OsIAA11 degradation in a manner dependent on the proteasome (27). These *in planta* and in vitro studies, together with demonstration of direct LRT2-catalyzed isomerization of the OsIAA11 degron motif by NMR (27), places this *cis–trans* molecular switch at a critical point in an important auxin-responsive circuit. Quantitative characterization of the LRT2/OsIAA11 reaction cycle would provide predictive power for understanding how this *cis–trans* molecular switch might serve as a timing device in a classic negative feedback circuit that controls lateral root development in rice, a well-studied phenotype with implications for food production.

Here, we have applied NMR to determine the microscopic thermodynamic and kinetic parameters of the four-state LRT2 reaction cycle acting on the W-P peptide bond in the OsIAA11 degron motif (Fig. 1*A*). NMR provides direct observation of *cis* and *trans* populations due to the slow timescale of interconversion which gives rise to distinct peaks, and enables determination of PPIase-catalyzed isomerization rates (28, 29). The detailed analysis of lineshapes in NMR titration experiments is a well-established method for extraction of information regarding mechanism, thermodynamics, and kinetics in protein–protein or protein–ligand interactions (30–32). Here, we used multidimensional lineshape analysis to determine the microscopic parameters that define the catalytic reaction cycle of LRT2 acting on the W-P peptide bond in the OsIAA11 degron motif. Notably, the full catalytic cycle for PPIase-catalyzed isomerization of a W-P peptide bond has not previously been characterized. We also have demonstrated that flanking regions do not significantly alter LRT2 activity on the core degron motif. The resulting catalytic cycle parameters provide predictive power for understanding this reaction at cellular concentrations, and for gaining critical insights regarding the utilization of an isomerase–substrate pair as a timing device in a developmental process. Given the high conservation of the cyclophilin active site and the degron sequence, these results have broad implications for predicting the activity of cyclophilins on Aux/IAA proteins in general.

Results

Determination of the Microscopic Parameters for LRT2 Catalysis of OsIAA11 Degron Motif. To quantify the thermodynamic and kinetic parameters that govern LRT2 catalysis of the WP peptide bond in the degron motif of OsIAA11, we applied NMR titration spectroscopy and lineshape analysis (28, 33). From the OsIAA11 perspective, this reaction can be modeled as a four-state thermodynamic cycle, with an equilibrium constant and forward and reverse rate constants for each of the four connecting steps (Fig. 1*A*). These equilibrium and rate constants provide a complete characterization of the catalytic reaction, enabling prediction of the overall exchange rate between free *trans* and *cis* isomers for any concentrations of LRT2 and OsIAA11.

The microscopic parameters associated with free OsIAA11 in the reaction cycle were first determined using apo ^{15}N-OsIAA11$^{72–125}$. The equilibrium constant, K_{eq}^{free}, was quantified using peak volumes corresponding to the well-resolved W104 indole H_N in *cis* and *trans* states in a 1D NMR spectrum of apo

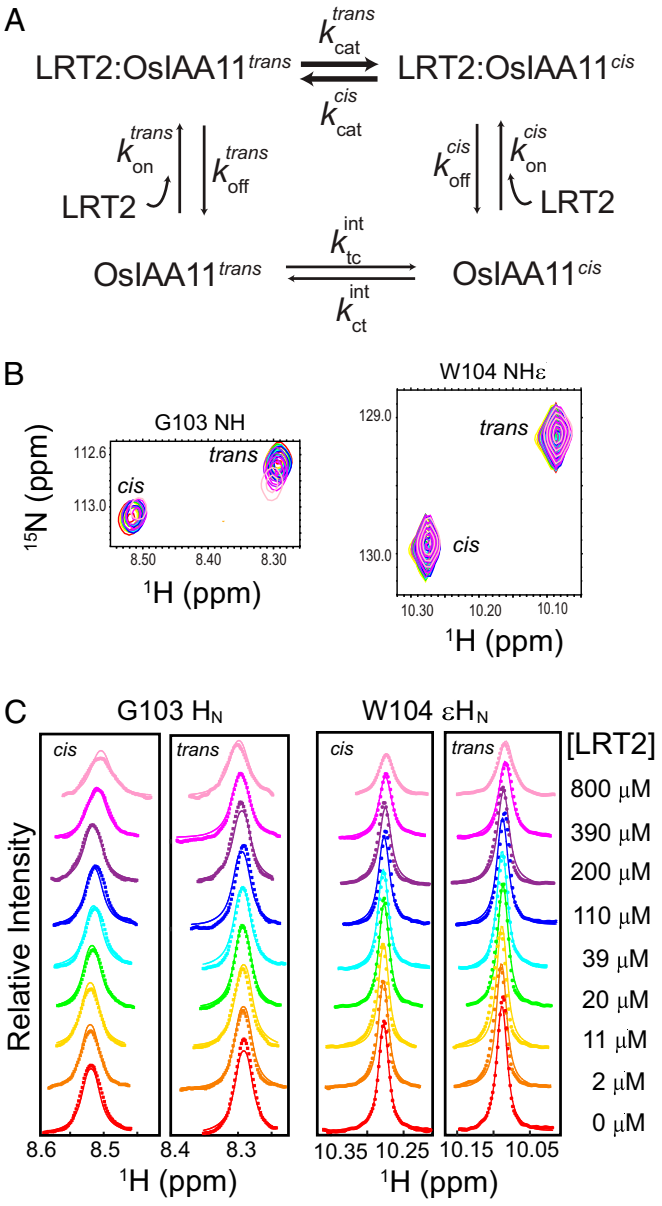

Fig. 1. Determination of four-state model parameters by lineshape analysis. (*A*) The four-state model for the LRT2/OsIAA11 reaction cycle and its associated microscopic parameters. (*B*) Expanded spectral regions of overlaid ^{15}N-^{1}H-HSQC spectra of 0.26 mM ^{15}N-labeled OsIAA11$^{72–125}$ with varying amounts of unlabeled LRT2 [0 mM (red) to 800 μM (pink)] showing resolved G103HN and W104-H$_N^{\varepsilon}$ peaks. (*C*) The ^{1}H peak simulations using the four-state model fitted microscopic parameters (*SI Appendix*, Table S1) and TITAN (33).

^{15}N-OsIAA11$^{72–125}$ acquired without saturation of water (*SI Appendix*, Fig. S1). The resulting value, $K_{eq}^{free} = 1.113$, reflects nearly equal *cis* (0.46) and *trans* (0.54) fractional populations, similar to reported values for W-P peptide bonds (11). Based on k_{ex}^{int} previously reported for W-P peptide bonds (11, 34), k_{ex}^{int} was set in simulations to 0.0008 s^{-1}. The precise k_{ex}^{int} value is not required for fitting, since the uncatalyzed isomerization is too slow to influence lineshapes (11). Individual peak chemical shifts and R_2 values for the free state (*SI Appendix*, Table S1) were obtained by fitting the apo 2D ^{1}H-^{15}N-HSQC spectrum of ^{15}N-OsIAA11$^{72–125}$ using Titration Analysis (TITAN) software (33).

To determine the remaining microscopic parameters for the reaction cycle, ^{15}N-OsIAA11$^{72–125}$ concentration was kept constant, and a reverse-titration with unlabeled LRT2 was performed to generate a series of 2D ^{1}H-^{15}N-HSQC spectra that were evaluated by lineshape analysis. The backbone N–H of G103 and the indole N–H of W104 give rise to well-resolved *trans* and *cis* peaks (Fig. 1*B*), providing two independent views of the isomerization reaction. Changes in position and lineshape of these peaks with varying LRT2 concentration were simulated and fit using TITAN (33) (Fig. 1*C* and *SI Appendix*, Fig. S2). Goodness of fit was insensitive to k_{off}^{cis} and k_{off}^{trans} when these values were >1,000 s^{-1}, and worsened when they were <1,000 s^{-1}, indicating that these dissociation rate constants are too fast to influence lineshapes (*SI Appendix*, Table S2). Thus, k_{off}^{cis} and k_{off}^{trans} were set at 17,000 s^{-1} and 15,000 s^{-1}, values consistent with a diffusion-limited on-rate (*SI Appendix*, Table S1) as described (28). Applying a bootstrap error analysis and simultaneously fitting the G103 and W104 peaks using TITAN, the optimized values $K_{eq}^{bound} = 1.119 \pm 0.110$, $K_d^{App} = 1.55 \pm 0.19$, and $k_{ex}^{cat} = 94.72 \pm 8$ were obtained along with the chemical shifts and R_2 values for the bound state of individual peaks (*SI Appendix*, Table S1). The corresponding affinities ($K_d^{cis} = K_d^{trans} = 1.55$ mM, obtained as described in *Materials and Methods*) are consistent with weak affinities reported for other PPIases (28). The LRT2:OsIAA11 reaction is strikingly balanced from a thermodynamic perspective, with nearly equal *cis* and *trans* affinities, and with both on-enzyme and free equilibrium constants near 1. Also notable is the on-enzyme exchange rate of ~95 Hz, which is 6- to 34-fold slower than values reported for other PPIase:substrate reactions (28, 29, 33). This slow exchange rate appears to be substrate-specific, since LRT2 displays typical cyclophilin activity on a standard cyclophilin peptide substrate (*SI Appendix*, Fig. S3).

Independent Validation of the Model and Fitted Microscopic Parameters. Independent validation of the four-state model and fitted parameters is important, since TITAN provides neither a mechanism for discriminating between models nor a rigorous approach for evaluating the accuracy of the fitted parameters. To independently measure the observed overall catalyzed exchange rate, k_{ex}^{obs} (Fig. 2*A*), the 2D ^{1}H-^{15}N heteronuclear (ZZ) exchange (Nzz) experiment was performed for a sample containing 0.8 mM ^{15}N-OsIAA11 and 16 μM LRT2. This measured rate can be compared with the predicted k_{ex}^{obs} value for the given sample concentrations (obtained as described in *Materials and Methods*). The peaks arising from the W104 indole N–H in the *cis* and *trans* states show distinct exchange cross-peaks only when LRT2 is present (Fig. 2*B*). Acquisition of a series of spectra with different mixing times and quantitative analysis of these auto- and cross-peak intensities as a function of mixing time allowed determination of k_{ex}^{obs} (Fig. 2 *C* and *D*). The resulting value, $k_{ex}^{obs} = 0.62$ s^{-2}, agrees well with the predicted value for these conditions, $k_{ex}^{obs} = 0.64$ s^{-1}. This shows that the model (Fig. 1*A*) and the fitted parameters (*SI Appendix*, Table S1) are able to accurately predict

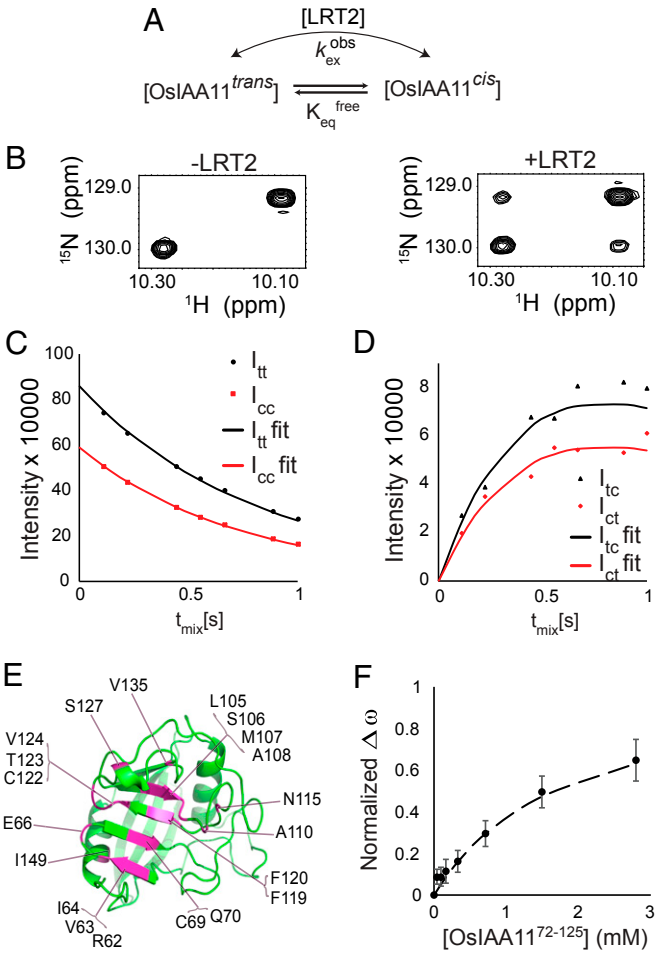

Fig. 2. Independent validation of model and fitted parameters. (*A*) Simplified schematic of LRT2/OsIAA11 reaction showing the observed exchange rate, k_{ex}^{obs}, measured using Nzz or ROESY experiments. (*B*) Region of ^{15}N-OsIAA11$^{72–125}$ Nzz spectrum showing W104-NHε *cis* and *trans* peaks at mixing time $t_{mix} = 0.55$ s, without LRT2 (*Left*) and with 16 μM LRT2 (*Right*). (*C* and *D*) Intensities of W104-NHε Nzz (*C*) autopeaks and (*D*) cross-peaks for 0.8 mM ^{15}N-OsIAA11$^{72–125}$ in the presence of 16 μM LRT2 as function of t_{mix}, fitted to obtain k_{ex}^{obs}. (*E*) Residues selected to determine K_d^{App} (magenta) mapped onto the LRT2 homology model. (*F*) Binding curve showing the average of the normalized chemical shift change ($\overline{\Delta\omega}$) induced by titration with unlabeled OsIAA11$^{72–125}$ over the selected 20 residues (dots) and the corresponding fitted curve (dashed line, $K_d^{App} = 1.54$ mM). Error bars denote the SD of Δω over the 20 residues at each titration point.

the experimentally observed exchange rate for a given sample condition.

For further validation, K_d^{App} was experimentally measured from the ^{15}N-LRT2 perspective. Of the 164 nonproline backbone peaks in the ^{15}N-LRT2 ^{1}H-^{15}N-HSQC spectrum, 20 have a significant composite chemical shift perturbation ($\Delta\omega$) when 2.79 mM OsIAA11$^{72–125}$ is added, and display trajectories that can be tracked throughout the titration (*SI Appendix*, Fig. S4). Significant change corresponds to $\Delta\omega \geq \overline{\Delta\omega} + \sigma$, where $\overline{\Delta\omega}$ is the average $\Delta\omega$ across the protein and σ is the SD (for this titration, $\overline{\Delta\omega} = 0.026$ ppm and $\sigma = 0.030$ ppm). Structural alignment of the LRT2 homology model (built as described in *Materials and Methods*) with human Cyclophilin A (CypA) shows that all of the selected 20 residues are located in or near the conserved cyclophilin binding region (Fig. 2*E*). These 20 residues were fit simultaneously using the built-in two-state model in TITAN, and a bootstrap error analysis was performed, yielding a well-fit

binding curve (Fig. 2*F*) with K_d^{App} = 1.54 ± 0.06 mM and k_{off} = 8,850 ± 2,350 s^{-1}, which agree fully with those derived above from lineshape analysis (K_d^{App} = 1.55 mM, k_{off}^{cis} and k_{off}^{trans} > 1,000 s^{-1}, *SI Appendix*, Table S2), providing further validation of the model and fitted parameters.

LRT2-Catalyzed Isomerization of OsIAA11 Degron Motif Is Not Altered by Upstream X-P Motifs. Interestingly, upstream of the degron motif in OsIAA11$^{72–125}$, there are four additional X-P motifs (Fig. 3*A*). To investigate their potential influence on LRT2 catalysis of the degron W-P, Pro-to-Ala mutagenesis was used to sequentially eliminate upstream X-P motifs (Fig. 3*A*). Application of the Nzz experiment to each ^{15}N-OsIAA11 mutant (0.8 mM) in the presence of LRT2 (16 μM) followed by data analysis (Fig. 3*B* and *SI Appendix*, Fig. S5) yields k_{ex}^{obs} values that are all highly similar to WT (ranging from 0.78 to 1.24 times WT; *SI Appendix*, Table S3), indicating that the additional X-P motifs do not alter significantly LRT2 catalysis of the W-P peptide bond in the degron motif of OsIAA11.

Peptide OsIAA11$^{98–109}$ Accurately Represents OsIAA11 as an LRT2 Substrate. Previous studies of LRT2 catalysis of the OsIAA11 degron motif have utilized a 12-residue peptide corresponding to OsIAA11 residues 98 to 109 (OsIAA11$^{98–109}$, Fig. 3*A*; ref. 27). The above results suggest that the fitted reaction parameters obtained using the longer OsIAA11$^{78–125}$ construct might accurately predict LRT2 binding and catalysis of OsIAA11$^{98–109}$. To investigate this, K_d^{App} was measured using ^{15}N-(6His)-LRT2 (without cleavage of the affinity tag) titrated with OsIAA11$^{98–109}$ (Fig. 4*A*), and k_{ex}^{obs} was measured using the rotating frame Overhauser effect spectroscopy (ROESY) experiment for a sample containing 1.84 mM OsIAA11$^{98–109}$ and 120 μM LRT2 (Fig. 4 *B* and *C*). The resulting K_d^{App} value (1.3 ± 0.4 mM) is within experimental error of K_d^{App} determined for OsIAA11$^{72–125}$ (1.54 ± 0.06 mM), demonstrating that the core degron sequence represents the complete LRT2 binding epitope. Moreover, the measured k_{ex}^{obs} value of 3.6 s^{-1} is in excellent agreement with the predicted value of 3.4 s^{-1} (obtained as described in *Materials and Methods*). The reported k_{ex}^{obs} value of 0.95 s^{-1} measured by ROESY for a sample containing 50 μM LRT2 and 2 mM OsIAA11$^{98–109}$ (27) is also reasonably predicted as 1.3 s^{-1}, despite different buffer conditions. These results demonstrate that the 12-residue degron peptide accurately represents the LRT2 substrate in OsIAA11$^{72–125}$, and suggest that the microscopic parameters determined here provide broad predictive power for conserved core degron sequences.

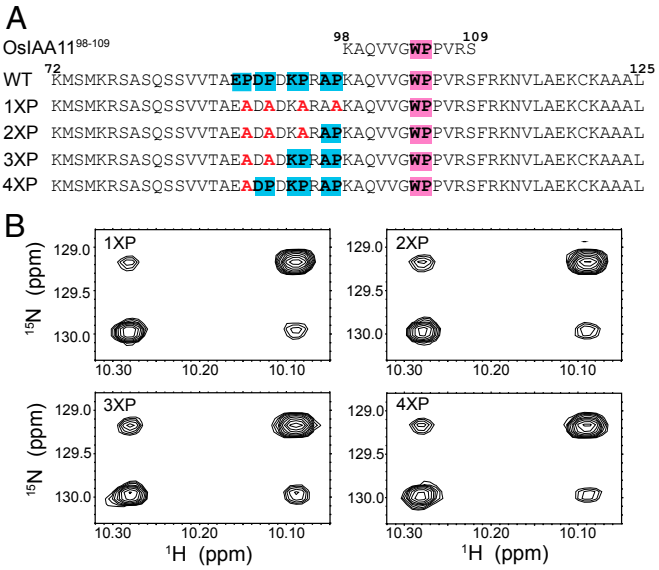

Fig. 3. Flanking X-P peptide bonds do not affect the isomerization of LRT2. (*A*) Sequences of the core OsIAA11 peptide, of OsIAA11 WT, and of OsIAA11 mutants designed to determine whether flanking X-P motifs (blue boxes) affect isomerization of the ^{104}W-P^{105} peptide bond (magenta box). KR (green box) is important for degradation rates of Aux/IAA proteins. (*B*) Expanded region of Nzz spectra of ^{15}N-OsIAA11$^{72–125}$ mutants in the presence of 16 μM LRT2 showing the W104-NHε peaks at mixing time of 0.55 s, demonstrating LRT2 catalysis of all four mutants.

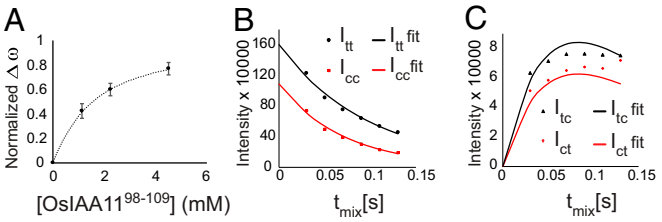

Fig. 4. Binding and isomerization of OsIAA11$^{78–109}$ by LRT2. (*A*) Binding curve showing $\overline{\Delta\omega}$ induced by titration with unlabeled OsIAA11$^{78–109}$ synthetic peptide for seven selected residues in ^{15}N-(6His)-LRT2 (dots) and the corresponding fitted curve (dashed line, K_d^{App} = 1.3 ± 0.4 mM). Error bars denote the SD in Δω over the seven residues at each titration point. The pH of this sample was 6.5. (*B* and *C*) Intensities of W104-NHε ROESY (*B*) autopeaks and (*C*) cross-peaks for 1.84 mM OsIAA11$^{78–109}$ in the presence of 120μM LRT2 as function of t_{mix}, fitted to obtain k_{ex}^{obs} for these sample conditions.

Discussion

The quantitative analysis of the reaction cycle for a given PPIase/substrate pair is a first step toward understanding the impact of this timing device in living cells and on phenotypes in whole organisms. Here, we have determined the microscopic equilibrium constants and kinetic rates for isomerization of the W-P degron motif in the transcription repressor OsIAA11 catalyzed by the rice cyclophilin LRT2. While LRT2 performs comparably to human CypA when acting on a standard cyclophilin substrate, LRT2 catalysis of the W-P peptide bond in the OsIAA11 degron motif is unusually slow. This work indicates that the W-P degron motif limits the on-enzyme isomerization rate, with a higher transition-state energy compared with the standard cyclophilin substrate. Since this is a complete characterization of the full reaction cycle for enzyme-catalyzed isomerization of a W-P peptide bond, these microscopic parameters provide important predictive power for understanding roles of W-P–based *cis–trans* timing devices, including the highly conserved degron motifs in plant gene regulation circuits.

While the NMR titration lineshape analysis studies reported here were necessarily performed at protein concentrations that far exceed the nanomolar to micromolar protein concentrations that can be reasonably expected in cells (35), our demonstration of the accurate prediction of independent measurements of k_{ex}^{obs} at different sample conditions indicates that the determined parameters are quite robust. Using these parameters and Eq. **3** (*Materials and Methods*), the predicted dependence of k_{ex}^{obs} on the concentrations of OsIAA11 and LRT2 ([OsIAA11] and [LRT2]) can be visualized (Fig. 5). Since the K_d value of 1.55 mM far exceeds the expected cellular [OsIAA11], k_{ex}^{obs} is independent of [OsIAA11] but is linearly dependent on [LRT2] (Eq. **3**). Based on the abundance of cyclophilins in human cells (35) and reported LRT2 mRNA levels in rice (36), a reasonable estimate of [LRT2] is 1 μM to 10 μM. The [OsIAA11] must necessarily vary between levels sufficiently high to shut down the transcription of its target genes and sufficiently low to turn them on

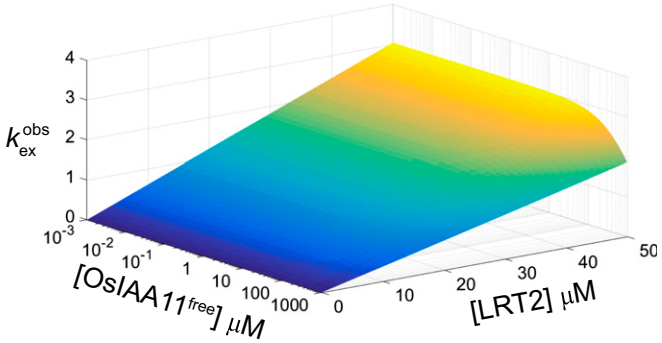

Fig. 5. Exchange rate as function of free OsIAA11$_{cis}$ and LRT2. The microscopic thermodynamic and kinetic parameters determined by NMR lineshape analysis predict an exchange rate linearly dependent on the LRT2 concentration, and invariant to OsIAA11 concentrations across a broad range (<1 mM).

(37–39). Thus, our NMR lineshape analysis predicts that the LRT2-catalyzed isomerization of OsIAA11 is an invariable step in the auxin circuit that maintains a constant k_{ex}^{obs} rate for a given [LRT2] over the wide range of [OsIAA11] encountered during the initiation of lateral root development.

The reaction parameters determined here reflect a highly balanced enzyme, with *cis–trans* equilibrium constants close to unity in both free (K_{eq}^{free}) and bound (K_{eq}^{bound}) forms. The on-enzyme equilibrium constant (K_{eq}^{bound}) has important implications for the catalytic effectiveness in the cell (40). An enzyme with $K_{eq}^{bound} = 1$ is optimized for the case where the ratio of the steady-state cellular concentrations of substrate and product, [S]/[P], is equal to their ratio at equilibrium, $[S]_{eq}/[P]_{eq}$. This happens when the next step in the pathway that depletes the product is much slower than the conversion of substrate to product. In the case of LRT2 and the auxin circuit, considering OsIAA11$_{trans}$ as the substrate and OsIAA11$_{cis}$ as the product specifically recognized by the SCF^{TIR1} E3 ubiquitin ligase, the next reaction is the ubiquitin-mediated proteasomal degradation of OsIAA11. The half-life of OsIAA11 has been approximated as 20 min (41), which corresponds to a rate of ~0.0006 s^{-1}. This suggests that, indeed, this slow degradation would allow LRT2 to maintain the steady-state [OsIAA11$_{trans}$] and [OsIAA11$_{cis}$] concentrations at equilibrium, corresponding to optimized catalytic effectiveness.

The studies presented here reveal that the level of LRT2 governs the isomerization rate for a broad range of OsIAA11 concentrations, and that LRT2 is optimized for its role in supplying OsIAA11$_{cis}$ to the proteasomal degradation pathway. Moreover, these results suggest that accelerating the isomerization reaction even further would not impact the auxin circuit, since the WT LRT2 reaction is much faster than the downstream degradation process that it feeds. Rather, tuning the LRT2 reaction to slower rates would potentially alter the circuit dynamics. Therefore, further studies of LRT2 mutants with diminished activities would be of particular interest for investigating the relationship between isomerization rate, auxin circuit dynamics, and phenotypic changes in lateral root development.

Materials and Methods

Plasmids, Proteins, and Peptides. LRT2 was purified as previously described (42), except that lysogeny broth media was used for expression of unlabeled protein, and M9 minimal media enriched only with $^{15}NH_4Cl$ was used for ^{15}N-labeled protein. All NMR samples were in 50 mM KCl, 100 mM KPO_4, 1 mM TCEP, 0.1% Halt Protease Inhibitor Mixture, EDTA free (Thermo Fisher Scientific), 5 mM NaN_3, and 8% D_2O, pH = 6.67.

The OsIAA11$^{72–125}$ gene was purchased from Genscript with a human rhinovirus-3C protease (3CPro) cleavage site at the N-terminal end. BamHI and HindIII cut sites were introduced via PCR. The PCR product was digested and then ligated into a pET28 vector with His6tag, tobacco etch virus protease cleavage site, and SUMO fusion protein at the N terminus. Four OsIAA11$^{72–125}$ mutants (Fig. 3*A*) were purchased in pET28a(+) vectors with the SUMO sequence, a 3CPro cleavage site, and the OsIAA11$^{72–125}$ sequence with the specified mutations (Fig. 3*A*). Expression and purification of OsIAA11$^{72–125}$ and its mutants were carried out as for LRT2, with the exception that 3CPro was used for cutting of His-SUMO tag for 48 h.

The OsIAA11$^{98–109}$ (acetyl-$_{98}$KAQVVGWPPVRS$_{109}$-amide) and the standard cyclophilin (acetyl-GSFGPDLRAGD-amide) natural abundance (not isotopically labeled) peptides were synthesized and HPLC-purified by Tufts Core Facility.

NMR Experiments and Analysis. All NMR experiments were performed at 25 °C on a Varian Inova 600-MHz spectrometer with a (H, C, N) Z-axis gradient probe. Spectra were processed and analyzed using nmrPipe (43), nmrdraw (43), Sparky (44), and TITAN (33). Free induction decays were apodized using an exponential or phase-shifted sine bell function and zero-filled before Fourier transformation. NMR acquisition and processing parameters are provided in *SI Appendix*. For all TITAN fittings, a bootstrap error with 100 replicas was carried out to obtain uncertainties in the fitted values.

For lineshape analysis titration experiments, ^{15}N-OsIAA11$^{72–125}$ was held at 0.26 mM, and unlabeled LRT2 was varied (0, 0.002, 0.011, 0.020, 0.039, 0.110, 0.200, 0.390, and 0.800 mM) by reverse titration. At each titration point, an ^{15}N-^{1}H HSQC spectrum (45) was acquired. The 2D lineshape analysis was performed using TITAN software (33). For ^{15}N-OsIAA11$^{72–125}$ titrated with LRT2, data were fit to the built-in four-state model, which considers the free and bound states of the *cis* and *trans* isomer. Fitted parameters include the on-enzyme equilibrium constant (K_{eq}^{bound}), the on-enzyme catalysis rate (k_{ex}^{cat}), the apparent affinity (K_d^{App}), the chemical shift of the bound state for each isomer, and the linewidths of the bound state of each isomer ($R_{2,0}^{bound}$). Constrained parameters include the equilibrium constant in the free state (K_{eq}^{free}), which was measure by 1D spectroscopy (*SI Appendix*, Fig. S1), the intrinsic exchange rate (k_{ex}^{int}), the chemical shift of the free state for each isomer, the linewidth of the free state ($R_{2,0}^{free}$), the reverse binding rates (k_{off}^{cis}, k_{off}^{trans}), and the scalar coupling values (6.5 Hz for G103-HN and 3 Hz for W104-NHε). The chemical shift of the free state and $R_{2,0}^{free}$ were fit for ^{15}N-OsIAA11$^{72–125}$ with 0 mM LRT2, and values obtained from this spectrum were used throughout the lineshape analysis. The intrinsic exchange rate (k_{ex}^{int}) was kept to 0.0008 s^{-1} as described in *Results* and elsewhere (11). The reverse binding rates were not deemed to be reliable extractable parameters; they were constrained assuming a diffusion limit on rate of ~10^7 $M^{-1}{\cdot}s^{-1}$. The affinities were calculated from the fitted parameters using the following equations:

$$K_d^{cis} = K_d^{App}\frac{\left(1+K_{eq}^{bound}\right)}{\left(1+K_{eq}^{free}\right)} \quad [1]$$

$$K_d^{trans} = K_d^{App}\frac{\left(K_{eq}^{free}\right)}{\left(K_{eq}^{bound}\right)}\frac{\left(1+K_{eq}^{bound}\right)}{\left(1+K_{eq}^{free}\right)}. \quad [2]$$

For independent measurement of K_d^{App}, ^{15}N-LRT2 (held at 0.235 mM) was titrated with varying concentrations of OsIAA11$^{72–125}$ protein (0, 0.04, 0.09, 0.17, 0.33, 0.71, 1.50, and 2.79 mM) by reverse titration. Protein concentrations were determined by UV absorbance based on their theoretical extinction coefficients, 10,220 $cm^{-1}{\cdot}M^{-1}$ and 5,500 $cm^{-1}{\cdot}M^{-1}$ at 280 nm for LRT2 and OsIAA11$^{72–125}$, respectively. At each titration point, an ^{15}N-^{1}H fast HSQC spectrum (46) was acquired. Intensities of the 20 selected peaks were fit using a built-in two-state model in TITAN to determined K_d^{App} and bound chemical shifts. Similarly, for measurement of K_d^{App} for OsIAA11$^{98–109}$, ^{15}N-(6His)-LRT2 concentration was held at 550 μM, and the OsIAA11$^{98–109}$ concentrations were 4.5, 2.25, 1.125, and 0 mM.

For measurements of k_{ex}^{obs}, Nzz (47, 48) and ROESY (49) experiments were performed. For Nzz experiments to measure k_{ex}^{obs} for LRT2-catalyzed W-P isomerization of ^{15}N-OsIAA11$^{72–125}$ WT and its mutants, samples containing 0.8 mM of ^{15}N-OsIAA11$^{72–125}$ (WT or mutant) with and without 16 μM LRT2 were prepared. A series of Nzz spectra with mixing times of 0.011, 0.11, 0.22, 0.44, 0.55, 0.67, 0.89, and 1.00 s were acquired. For ROESY experiments to measure the k_{ex}^{obs} for LRT2-catalyzed W-P isomerization of OsIAA11$^{98–109}$, LRT2 concentration was 120 μM, and OsIAA11$^{98–109}$ concentration was 1.84 mM. ROESY experiments were run with mixing times of 30, 50, 70, 90, 110, and 130 ms. Nzz and ROESY peak heights for autopeaks and cross-peaks corresponding to the indole proton in W104 were obtained using Sparky (44). Peak intensities were fit to obtain k_{ex}^{obs} as described elsewhere (28, 50).

The measured k_{ex}^{obs} value can be compared with the predicted value based on the four-state model parameters and sample conditions using the reversible Michaelis–Menten equation (28),

$$k_{ex}^{obs} = \left(\frac{k_{cat}^{trans}}{K_d^{trans}} + \frac{k_{cat}^{cis}}{K_d^{cis}}\right) \frac{[E]^{total}}{1 + \frac{[trans]^{free}}{K_d^{trans}} + \frac{[cis]^{free}}{K_d^{cis}}}, \quad [3]$$

where $[E]^{total}$ is the total enzyme concentration, while $[trans]^{free}$ and $[cis]^{free}$ are the concentrations of the indicated isomer in the free state.

Homology Model Construction. The LRT2 amino acid sequence is 87.7% identical to wheat cyclophilin TaCypA-1, the closest homolog for which a structure is determined [Protein Data Bank ID 4hy7.1 (51)]. Using 4hy7.1 as a template, a high-quality (QMEAN = 0.95, GMQE = 0.95) LRT2 homology model was constructed using SWISS MODEL (52).

ACKNOWLEDGMENTS. This work was supported by National Science Foundation Grant MCB-1615350 and by the National Institutes of Health under Ruth L. Kirschstein National Research Service Award 2T32GM008267 from the National Institute of General Medical Sciences.

1. Christoforides E, Dimou M, Katinakis P, Bethanis K, Karpusas M (2012) Structure of a bacterial cytoplasmic cyclophilin A in complex with a tetrapeptide. *Acta Crystallogr Sect F Struct Biol Cryst Commun* 68:259–264.
2. Davis TL, et al. (2010) Structural and biochemical characterization of the human cyclophilin family of peptidyl-prolyl isomerases. *PLoS Biol* 8:e1000439.
3. Göthel SF, Marahiel MA (1999) Peptidyl-prolyl cis-trans isomerases, a superfamily of ubiquitous folding catalysts. *Cell Mol Life Sci* 55:423–436.
4. Lu KP, Finn G, Lee TH, Nicholson LK (2007) Prolyl cis-trans isomerization as a molecular timer. *Nat Chem Biol* 3:619–629.
5. Fischer G, Aumüller T (2003) Regulation of peptide bond cis/trans isomerization by enzyme catalysis and its implication in physiological processes. *Rev Physiol Biochem Pharmacol* 148:105–150.
6. Hanes SD (2015) Prolyl isomerases in gene transcription. *Biochim Biophys Acta* 1850: 2017–2034.
7. Perrucci GL, et al. (2015) Peptidyl-prolyl isomerases: A full cast of critical actors in cardiovascular diseases. *Cardiovasc Res* 106:353–364.
8. Kumari S, Roy S, Singh P, Singla-Pareek SL, Pareek A (2013) Cyclophilins: Proteins in search of function. *Plant Signal Behav* 8:e22734.
9. Kang B, et al. (2013) OsCYP2, a chaperone involved in degradation of auxin-responsive proteins, plays crucial roles in rice lateral root initiation. *Plant J* 74:86–97.
10. Williamson MP (1994) The structure and function of proline-rich regions in proteins. *Biochem J* 297:249–260.
11. Reimer U, et al. (1998) Side-chain effects on peptidyl-prolyl cis/trans isomerisation. *J Mol Biol* 279:449–460.
12. Hamelberg D, McCammon JA (2009) Mechanistic insight into the role of transition-state stabilization in cyclophilin A. *J Am Chem Soc* 131:147–152.
13. Papin JA, Hunter T, Palsson BO, Subramaniam S (2005) Reconstruction of cellular signalling networks and analysis of their properties. *Nat Rev Mol Cell Biol* 6:99–111.
14. Tan X, et al. (2007) Mechanism of auxin perception by the TIR1 ubiquitin ligase. *Nature* 446:640–645.
15. Gray WM, Kepinski S, Rouse D, Leyser O, Estelle M (2001) Auxin regulates SCF(TIR1)-dependent degradation of AUX/IAA proteins. *Nature* 414:271–276.
16. Tiwari SB, Wang XJ, Hagen G, Guilfoyle TJ (2001) AUX/IAA proteins are active repressors, and their stability and activity are modulated by auxin. *Plant Cell* 13: 2809–2822.
17. Normanly J (2010) Approaching cellular and molecular resolution of auxin biosynthesis and metabolism. *Cold Spring Harb Perspect Biol* 2:a001594.
18. Del Pozo JC, Manzano C (2014) Auxin and the ubiquitin pathway. Two players-one target: The cell cycle in action. *J Exp Bot* 65:2617–2632.
19. Liscum E, Reed JW (2002) Genetics of Aux/IAA and ARF action in plant growth and development. *Plant Mol Biol* 49:387–400.
20. Ramos JA, Zenser N, Leyser O, Callis J (2001) Rapid degradation of auxin/indoleacetic acid proteins requires conserved amino acids of domain II and is proteasome dependent. *Plant Cell* 13:2349–2360.
21. Mockaitis K, Estelle M (2008) Auxin receptors and plant development: A new signaling paradigm. *Annu Rev Cell Dev Biol* 24:55–80.
22. Reed JW (2001) Roles and activities of Aux/IAA proteins in arabidopsis. *Trends Plant Sci* 6:420–425.
23. Hagen G, Guilfoyle T (2002) Auxin-responsive gene expression: Genes, promoters and regulatory factors. *Plant Mol Biol* 49:373–385.
24. Hayashi K (2012) The interaction and integration of auxin signaling components. *Plant Cell Physiol* 53:965–975.
25. Zhu ZX, et al. (2012) A gain-of-function mutation in OsIAA11 affects lateral root development in rice. *Mol Plant* 5:154–161.
26. Zheng H, et al. (2013) LATERAL ROOTLESS2, a cyclophilin protein, regulates lateral root initiation and auxin signaling pathway in rice. *Mol Plant* 6:1719–1721.
27. Jing H, et al. (2015) Peptidyl-prolyl isomerization targets rice Aux/IAAs for proteasomal degradation during auxin signalling. *Nat Commun* 6:7395.
28. Greenwood AI, et al. (2011) Complete determination of the Pin1 catalytic domain thermodynamic cycle by NMR lineshape analysis. *J Biomol NMR* 51:21–34.
29. Holliday MJ, Armstrong GS, Eisenmesser EZ (2015) Determination of the full catalytic cycle among multiple cyclophilin family members and limitations on the application of CPMG-RD in reversible catalytic systems. *Biochemistry* 54:5815–5827.
30. Acevedo LA, Greenwood AI, Nicholson LK (2017) A noncanonical binding site in the EVH1 domain of vasodilator-stimulated phosphoprotein regulates its interactions with the proline rich region of zyxin. *Biochemistry* 56:4626–4636.
31. Rennie ML, Doolan AM, Raston CL, Crowley PB (2017) Protein dimerization on a phosphonated calix[6]arene disc. *Angew Chem Int Ed Engl* 56:5517–5521.
32. Shinya S, et al. (2017) NMR line shape analysis of a multi-state ligand binding mechanism in chitosanase. *J Biomol NMR* 67:309–319.
33. Waudby CA, Ramos A, Cabrita LD, Christodoulou J (2016) Two-dimensional NMR lineshape analysis. *Sci Rep* 6:24826.
34. Greenwood AI, Kwon J, Nicholson LK (2014) Isomerase-catalyzed binding of interleukin-1 receptor-associated kinase 1 to the EVH1 domain of vasodilator-stimulated phosphoprotein. *Biochemistry* 53:3593–3607.
35. Beck M, et al. (2011) The quantitative proteome of a human cell line. *Mol Syst Biol* 7: 549.
36. Kawahara Y, et al. (2013) Improvement of the *Oryza sativa* Nipponbare reference genome using next generation sequence and optical map data. *Rice (N Y)* 6:4.
37. Farcot E, Lavedrine C, Vernoux T (2015) A modular analysis of the auxin signalling network. *PLoS One* 10:e0122231.
38. Middleton AM, King JR, Bennett MJ, Owen MR (2010) Mathematical modelling of the Aux/IAA negative feedback loop. *Bull Math Biol* 72:1383–1407.
39. Vernoux T, et al. (2011) The auxin signalling network translates dynamic input into robust patterning at the shoot apex. *Mol Syst Biol* 7:508.
40. Burbaum JJ, Raines RT, Albery WJ, Knowles JR (1989) Evolutionary optimization of the catalytic effectiveness of an enzyme. *Biochemistry* 28:9293–9305.
41. Moss BL, et al. (2015) Rate motifs tune auxin/indole-3-acetic acid degradation dynamics. *Plant Physiol* 169:803–813.
42. Acevedo LA, Nicholson LK (2018) ^{1}H, ^{13}C and ^{15}N NMR assignments of cyclophilin LRT2 (OsCYP2) from rice. *Biomol NMR Assign* 12:171–174.
43. Delaglio F, et al. (1995) NMRPipe: A multidimensional spectral processing system based on UNIX pipes. *J Biomol NMR* 6:277–293.
44. Goddard TD, Kneller DG (2008) *Sparky 3* (Univ California, San Francisco).
45. Mulder FA, Spronk CA, Slijper M, Kaptein R, Boelens R (1996) Improved HSQC experiments for the observation of exchange broadened signals. *J Biomol NMR* 8: 223–228.
46. Mulder FA, Schipper D, Bott R, Boelens R (1999) Altered flexibility in the substrate-binding site of related native and engineered high-alkaline *Bacillus subtilisins*. *J Mol Biol* 292:111–123.
47. Farrow NA, Zhang O, Forman-Kay JD, Kay LE (1994) A heteronuclear correlation experiment for simultaneous determination of ^{15}N longitudinal decay and chemical exchange rates of systems in slow equilibrium. *J Biomol NMR* 4:727–734.
48. Montelione GT, Wagner G (1989) 2D chemical exchange NMR spectroscopy by proton-detected heteronuclear correlation. *J Am Chem Soc* 111:3096–3098.
49. Bax A & Davis DG (1985) Practical aspects of two-dimensional transverse NOE spectroscopy. *J Magn Reson (1969)* 63:207–213.
50. Nechama M, et al. (2018) The IL-33-PIN1-IRAK-M axis is critical for type 2 immunity in IL-33-induced allergic airway inflammation. *Nat Commun* 9:1603.
51. Sekhon SS, et al. (2013) Structural and biochemical characterization of the cytosolic wheat cyclophilin TaCypA-1. *Acta Crystallogr D Biol Crystallogr* 69:555–563.
52. Waterhouse A, et al. (2018) SWISS-MODEL: Homology modelling of protein structures and complexes. *Nucleic Acids Res* 46:W296–W303.